FRONTIERS OF PHYSICS

RESEARCH ARTICLE
Volume 18 / Issue 2 / 23301 / 2023

Electronic properties and tunability in graphene/3D-InP mixed-dimensional van der Waals heterostructure

Qingyun Zhou, Yusheng Hou†, Tianshu Lai‡

School of Physics, State Key Lab. of Optoelectronic Materials and Technologies, Sun Yat-Sen University, Guangzhou 510275, China
Corresponding authors. E-mail: †houysh@mail.sysu.edu.cn, ‡stslts@mail.sysu.edu.cn
Received June 13, 2022; accepted October 2, 2022

© Higher Education Press 2023

ABSTRACT

InP solar cell is promising for space application due to its strong space radiation resistance and high power conversion efficient (PCE). Graphene/InP heterostructure solar cell is expected to have a higher PCE because strong near-infrared light can also be absorbed and converted additionally by graphene in this heterostructure. However, a low PCE was reported experimentally for Graphene/InP heterostructures. In this paper, electronic properties of graphene/InP heterostructures are calculated using density functional theory to understand the origin of the low PCE and propose possible improving ways. Our calculation results reveal that graphene contact with InP form a p-type Schottky heterostructure with a low Schottky barrier height (SBH). It is the low SBH that leads to the low PCE of graphene/InP heterostructure solar cells. A new heterostructure, graphene/insulating layer/InP solar cells, is proposed to raise SBH and PCE. Moreover, we also find that the opened bandgap of graphene and SBH in graphene/InP heterostructures can be tuned by exerting an electric field, which is useful for photodetector of graphene/InP heterostructures.

Keywords graphene, InP(III), heterostructure, density functional theory

1 Introduction

Graphene, a two dimensional (2D) atomically thin monolayer, has been widely applied in electronic and optoelectronic devices due to its unique electronic properties, such as the high mobility and diffusion coefficient [1, 2], 97.7% optical transmittance in a wide spectrum range [3] and outstanding thermal conductivity [4]. However, its zero band gap [5] has limited its applications in devices. To improve the performance of graphene, a lot of schemes have been proposed to open its band gap, such as mechanical strain [6], external electric field [7, 8] and layer stacking [9–12]. Especially, a layer stacking between graphene and another semiconductors, which forms a Schottky junction and tunes band gap of graphene, is a promising practical method that attracts widespread attention in devices design [13–15]. Recently, graphene-based semiconductor heterostructure through van der Waals (vdW) interaction have been fabricated experimentally and investigated theoretically, such as graphene/TMDCs (2D transition-metal dichalcogenides) [16–18], graphene/g-GaN [19, 20], and graphene/InAs [21, 22]. They were demonstrated more advancing properties and potential application than the single material form.

Semiconductor InP is a potential material for a high conversion efficiency solar cell due to its direct bandgap of 1.42 eV [23], which locates at the optimum energy range of solar energy spectrum [24]. In addition, compared to the extensive use of Si and GaAs semiconductors in solar cell [25–27], InP solar cell is promising for space application due to its high resistance to space radiation damage [28]. Therefore, graphene/InP Schottky junction is considered as a promising optoelectronic junction device due to its high resistance to space irradiation [29]. Especially, the power conversion efficiency

Higher Education Press

https://doi.org/10.1007/s11467-022-1224-8

(PCE) of ~23%, close to PCE of GaAs solar cell, is theoretically predicted for InP under AM0 (air mass) illumination [28], while PCE of 16.5% was experimentally reported for InP homojunction solar cell under AM1.5 [28]. A higher PCE of 18.5% was reported for graphene/GaAs heterojunction solar cell [27]. However, only a low PCE of 5.6% was reported for graphene/InP heterojunction solar cell [29]. The origin of such a low PCE for graphene/InP heterojunction solar cells could not been understood based on reported theoretical calculations on electronic properties of graphene/2D-InP heterostructure [30] because a real graphene/InP solar cell was graphene contact on top of a bulk InP slab [29, 31]. Therefore, it is very necessary to investigate the interfacial interaction between graphene and bulk InP and to understand electronic properties as well as Schottky barrier height (SBH) in graphene/3D-InP heterojunction.

In this work, graphene/3D-InP(111) heterostructure is constructed. Three stable heterostructures with the different binding sites of graphene on InP(111) slab are found. Their interfacial interaction, electronic properties and the effect of electric field are studied in detail by density functional theory (DFT) calculations. We find that the band structures of these heterostructures basically preserve sole electronic properties of graphene and InP(111) slab due to the weak vdW force interaction between graphene and InP(111) slab. A built-in electric field exists in the interface of these heterostructures, and points to InP slab from graphene. Furthermore, graphene/InP heterostructure forms a p-type Schottky contact that has a low SBH. It is the low SBH that may result in low PCE of graphene/3D-InP heterostructure solar cells. A new heterostructure, graphene/insulating layer/InP solar cell is proposed to increase SBH and PCE. We also find that graphene opens up a small bandgap in graphene/3D-InP heterostructures, and the bandgap can be tuned by an external electrical field applied perpendicularly to the interface. The tunable bandgap may be useful for the applications of photoelectronic detectors of graphene/InP heterojunctions.

2 Computational methods

Our DFT calculations are performed using the projector augment wave (PAW) [32] method as implemented in the Vienna *ab initio* Simulation Package (VASP) [33]. The electronic exchange correlation energy is treated by the generalized-gradient approximation (GGA) of Perdew–Burke–Ernzerhof (PBE) [34]. In order to accurately describe the vdW interactions between graphene and InP, the DFT-D2 method of Grimme [35] is adopted because it has a similar effect to GGA+DFT-D3 method, whereas GGA has an anomalous effect, as reported previously [36]. The k-point sampling in the first Brillouin zone is implemented by the Monkhorst-Pack scheme with the grids of 3 × 3 × 1 for graphene/InP heterostructures. The cutoff energy for plane wave basis expansion is set as 400 eV, and the convergence criteria of energy and force reach 10^{-5} eV and 0.02 eV·Å^{-1}, respectively.

Before the graphene/InP heterojunctions are constructed, we first investigate the graphene monolayer, InP bulk, and InP slab. Here, we only take account for InP with the zinc blend phase because it is stable under room temperature. The optimized lattice parameters are $a = b = 2.46$ Å for graphene, and $a = b = 5.869$ Å for InP, being in a good agreement with experimentally reported values ($a = b = 5.868$ Å for InP [37]). To minimize the lattice mismatch between the stacking sheets, a $(2\sqrt{3} \times 2\sqrt{3})$R30° -graphene supercell is stacked on a (2×2)-reconstructed InP surface, which lead to a lattice mismatch 2.7% between graphene and InP. In the following calculations, this lattice mismatch is processed by compressing the lattice constant of graphene by 2.7% because the electronic properties of graphene is robust against compressive strain [19]. The InP surface is modeled by a slab geometry with six double layer InP and a 25 Å vacuum layer. Note that this InP slab contains 12 layers which are the integer number of irreducible crystalline layers [38]. P atoms at the bottom surfaces of InP slab are terminated by artificial hydrogen atoms with fractional charges of 0.75e [39, 40]. InP surface is (2 × 2) unit cell and can be directly cleave from InP bulk, and contain an In vacancy per (2 × 2) unit cell [41, 42]. The In vacancy is a cation vacancy, which fulfills the electron counting rule [43]. The geometry of graphene/InP heterojunction is optimized with the upper four layers of InP slabs being fully relaxed while the remaining layers are consistent with bulk phase. The above-mentioned structures of $(2\sqrt{3} \times 2\sqrt{3})$R30°-graphene supercell and (2×2)-reconstructed InP surface are shown in Figs. 1(a) and (b).

3 Results and discussion

3.1 Geometry and stability of graphene/InP heterostructures

Based on the stacking position of the graphene layer on InP slab, three possible configurations of graphene/InP heterostructures may be formed, as shown in Fig. 1(c) by A, B and C. The graphene/InP heterostructure has three possible binding sites for both In and P atoms on graphene: (i) on a top site (configuration A), i.e., directly above a carbon atom, (ii) on a hollow site (configuration B), which is the center of the carbon honeycomb, and (iii) at the midpoint sites of the carbon-carbon bridge (configuration C). We have calculated the total energies of the three heterojunction configurations as a function of distance d_0 between InP slab and monolayer graphene. For any d_0, the total energy of configuration

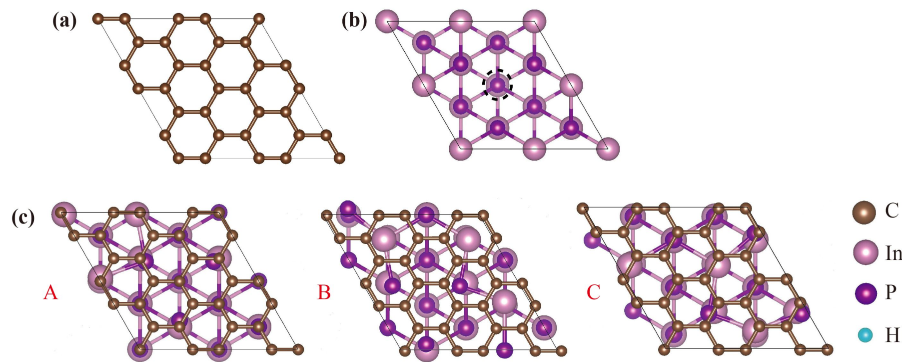

Fig. 1 The top view of **(a)** $2\sqrt{3}\times2\sqrt{3}$-graphene and **(b)** 2×2-InP(111). **(c)** The top view of the graphene/InP heterostructure. Brown, pink, violet, and blue color circles represent the atoms of C, In, P, and H, respectively. The dash circle represents the position of vacancy.

A and C are very close and always lower than configuration B, which suggests that the absorption sites of the top and bridge are the energetically favorable stacking configurations. As listed in Table I, the optimum interfacial distance by minimizing the total energy is 3.16 Å, 3.24 Å, and 3.19 Å for configurations A, B, and C, respectively. Such an interlayer distance of roughly 3.2 Å is much larger than the summation of the covalent radii of C and In or P atom (0.75 Å for C atom, 1.66 Å for In atom and 1.0 Å for P atom) [30], clearly indicating a physical adsorption between graphene and InP monolayers.

The thermodynamic stability of the graphene/InP heterojunctions can be described by binding energy, which is obtained according to the following equation:

$$E_b=(E_{\text{graphene/InP}}-E_{\text{graphene}}-E_{\text{InP}})/S, \tag{1}$$

where $E_{\text{graphene/InP}}$, E_{graphene}, and E_{InP} represent the energies of the graphene/InP heterostructure, monolayer graphene and InP slab, respectively. In Eq. (1), S is the surface area of graphene/InP heterojunction. According to this definition, we can obtain that binding energies (E_{b}) of the three configurations A, B, and C are –61.8, –59.7, and –61.6 meV/Å^2 (Table 1), respectively. These negative binding energies imply that graphene and InP slab can form a thermodynamically stable graphene/InP heterostructure.

To qualitatively reveal the bonding mechanism between graphene and InP slab in graphene/InP, electron local function (ELFs) of the three stacking configurations with the equilibrium distance are calculated and shown in Figs. 2 (a)–(c). The red color represents completely localized electrons, while the blue represents completely delocalized electrons. It is obvious that the electrons in the heterostructure are localized to the C-C bond in graphene and P atom in InP(111) to a large extent. Owing to the large layer spacing, there are almost no electrons localized between graphene and InP slab, which implies that graphene and InP slab in all configurations are not bonded chemically, but mainly physical adsorptions.

3.2 Electronic properties of graphene/InP heterostructures

First, the band structures of sole graphene and InP slab as well as their heterostructures and projected density of states of the heterostructure are calculated and plotted in Fig. 3. From Fig. 3(a), we can see that the linear dispersive Dirac cone of $2\sqrt{3}\times2\sqrt{3}$-supercell graphene is folded to Γ point from the original K point, consistent with a previous report [44]. Figure 3(b) shows the band structure of InP slab with a direct band gap of 0.889 eV occurring at Γ point.

The evolution of the band structures of graphene/InP heterostructures with different configuration are shown in Figs. 3(c)–(e). The red filled circles represent the band states of graphene, while the black solid line represents those of InP slab. Comparing the band structures of the isolated graphene and InP slab as shown in Fig. 3(a), it is clear that the electronic properties of isolated graphene and InP slab are mostly preserved in the heterostructures due to the weak vdW interaction, although there is a weak hybridization between the π^*

Table 1 Listed are the equilibrium interlayer distance d_0 (Å), binding energy E_{b} of graphene/InP heterostructure, opened band gap E_{g} of graphene in the heterostructure, the work function W of InP slab and graphene, and Schottky barrier heights (Φ_{p} , Φ_{n}) of graphene/InP heterostructure.

Graphene/InP		d_0 (Å)	E_{b} (meV/Å^2)	E_{g} (meV)	W (eV)	Φ_{p} (meV)	Φ_{n} (eV)
	A	3.16	–61.8	73.1	4.23 (graphene)	22.2	0.850
Configuration	B	3.24	–59.7	170.9	4.31 (InP slab)	85.5	0.729
	C	3.19	–61.6	81.3	–	41.1	0.882

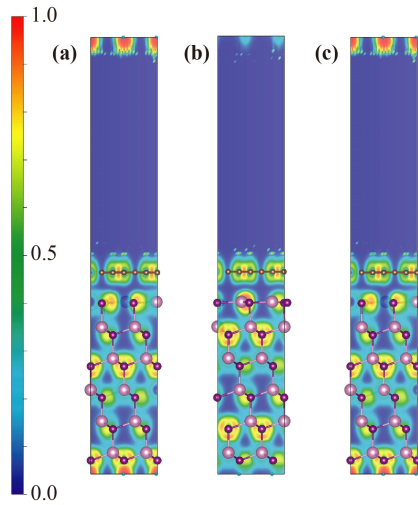

Fig. 2 Electronic localization functions (ELF) of graphene/InP heterostructure. **(a)** Configuration A, **(b)** configuration B and **(c)** configuration C. The top crystal structure is graphene, while the bottom is InP slab.

(antibonding) band of graphene and valence band edge of InP slab. In Figs. 3(c)–(e), one also finds that within the gap of InP slab, the bands have a predominant carbon character. Moreover, due to the proximity effects between InP slab and graphene, Dirac cones in heterostructures are opened a band gap. It is clear that different binding sites for graphene on InP(111) give rise to a direct band gap of 73.1, 170.9 and 81.3 meV (seen in Figs. 3(c)–(e) or Table 1) in graphene for configuration A, B and C, respectively. The physical origin of the appearance of band gap in graphene for graphene/InP heterostructures may be considered as the effect of the ionic potential of InP slab on the graphene layer. In this case, the on-site energies of the two sublattice of graphene are different, thus resulting in a band gap opening at the Dirac points. Similar phenomenon was also reported in graphene/Ga_2SSe heterostructure [45].

From Figs. 3(c)–(e), we can find that the Fermi level of these heterostructures are located within the band gap of InP slab, forming a Schottky heterostructure. According to the Schottky–Mott rule [46], the Schottky barrier heights are determined by the difference between the conduction band minimum or valence band maximum of InP slab and graphene's Fermi level. In these graphene/InP heterostructures, the n-type SBH is defined as $\Phi_n = E_{CBM} - E_F$, whereas the p-type SBH is defined as $\Phi_p = E_F - E_{VBM}$. The values of these SBH (Φ_n and Φ_p) are listed in Table 1. Our result show that the configuration A, B, and C form a p-type Schottky contact with $\Phi_p = 22.2$, 85.5, and 41.1 meV, respectively. These Φ_p are below 100 meV and very low. We speculate just the low SBH leads to a low PCE of graphene/3D-InP heterostructure solar cells because a low SBH in Schottky junction devices is unfavorable to separation of photogenerated electron-hole pairs.

To deeply understand the interface electronic structures in graphene/InP, the total density of state (TDOS) and projected density of state (PDOS) of configuration A, B and C are plotted in right panels of Figs. 3(c)–(e). One can see that around the Fermi level, the distribution of PDOS (green dashed dot line) of InP slab in any heterostructure almost agrees with the one of TDOS (black solid line) of the corresponding graphene/InP heterostructure, while the PDOS (red dashed line) of graphene is much weaker than the PDOSs of InP slabs,

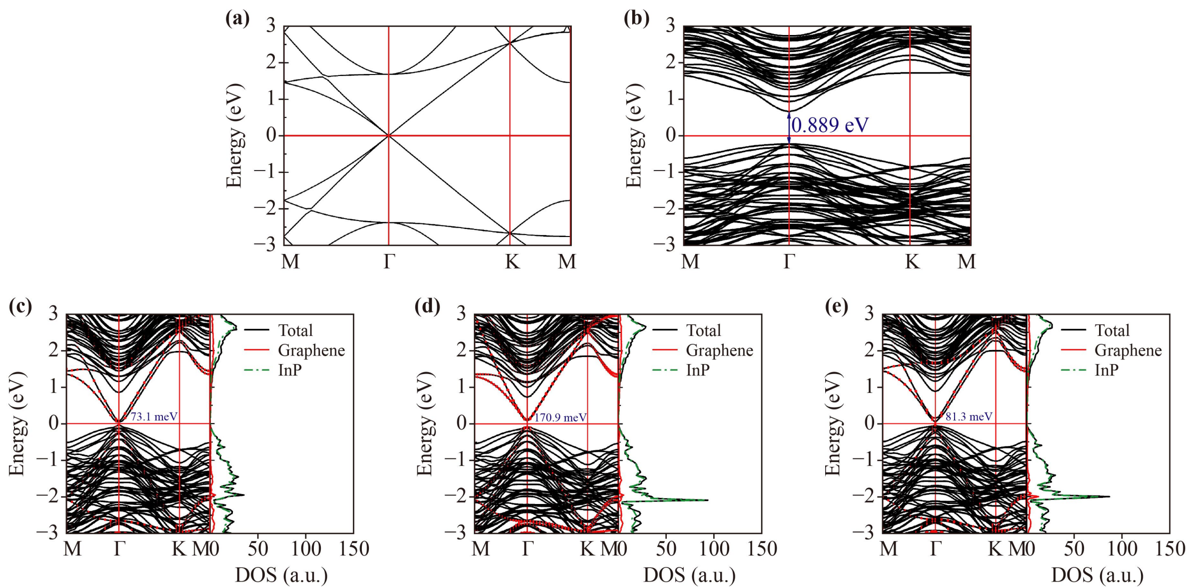

Fig. 3 The band structure of **(a)** isolated $2\sqrt{3}\times 2\sqrt{3}$-supercell graphene and **(b)** InP slab, Projected band structures and projected density of states of graphene/InP heterostructure: configurations **(c)** A, **(d)** B, **(e)** C. In (c)–(e), red filled circle represents the band structure of graphene. The Fermi level is set to zero.

which suggest that InP contributes dominantly to the TDOS of the corresponding graphene/InP heterostructures.

To obtain the charge distribution in the heterostructure, charge density difference is calculated to explore the charge transfer and separation at the graphene/InP interface. Here, charge density difference is defined as $\Delta\rho = \rho\,(\text{graphene/InP}) - \rho\,(\text{InP}) - \rho\,(\text{graphene})$, where $\rho\,(\text{graphene/InP})$, $\rho\,(\text{InP})$, $\rho\,(\text{graphene})$ are the charge densities of graphene/InP heterostructure, InP slab, and graphene, respectively. Figure 4 shows that these heterostructures have the same trend of charge redistributions. Charge redistribution mainly occurs near the graphene/InP interface, and is almost unobservable beyond the second double layer of InP. Such a result is mainly attributed to the weak vdW interaction between graphene and InP because this charge redistribution is much weaker and only occurs at interface between graphene and InP when vdW interaction is ignored.

The planar averaged charge density difference along the Z direction (the normal of the interface) are shown in the bottom panels in Fig. 4. For all graphene/InP heterostructures, we can observe charge depletion in the graphene side of the interface and charge accumulation near the surface of InP slab, which causes a built-in electric field whose direction points to InP slab from graphene. With the assistance of the built-in field, the photoelectrons in InP slab can be easily transported into graphene.

As we all know, the work function of the materials may assist to elucidate the charge transfer mechanism. Thus, we calculate the work function W (W is the energy difference between the vacuum level E_{vac} and E_{F}) of graphene and InP slab and summarize them in Table 1. The calculated W's of graphene and InP(111) are 4.23 eV and 4.30 eV, respectively. This indicates that the electrons will flow from the graphene to InP slab when they form a heterostructure. This result agrees with the analysis of charge density difference in Fig. 4.

Graphene/InP heterostructure would unavoidably be affected by external electric fields when it is used as photodetectors. It is also known that gate voltage is a valid way to control SBH [47]. Thus, it is important to explore the effect of an external electric field on the band structures of these heterojunctions. A vertical external electric field is applied to the interface of graphene/InP heterostructures, and the direction from InP(111) to graphene is defined as the positive. For the sake of simplification, we only take into account configuration A to further elucidate the electronic properties and SBH of graphene/InP at different values of bias voltage because other configurations B and C have similar performances to configuration A. In Fig. 5(a), we show the variation of opened band gap of graphene in the heterostructures with a perpendicular electric field by the solid triangles. One can find that the opened band gap in configurations A decreases with increasing the positive external electric field, while it increases slowly first and then decreases with increasing the negative external electric field. Therefore, the opened band gap of graphene can be significantly tunable from 36.7 mV to 78.3 meV as bias electric field decreases from 0.4 V/Å to –0.1 V/Å. Such a tunability of the opened band gap in graphene originates from interfacial interacting potential from InP tuned by the external electric fields applied, as discussed in Ref. [45]. This tunability of opened band gap of graphene may be useful for the applications of photodetectors of graphene/InP junctions.

We also calculate the band structures of the three stacking configurations at different bias voltages. For the sake of simplification, we only illustrate in Fig. 5(c) the band structure of configuration A at different values of bias voltage because other configuration B and C have similar performance to configuration A. From Fig. 5(c), one can clearly see that under a negative bias voltage, both Φ_{n} (yellow stripe) and Φ_{p} of the heterostructures are almost insensitive to the external electric field.

We calculate the variation of SBH with a bias voltage. The SBH is plotted as a function of the bias electric field in Fig. 5(b) for configurations A. It is obvious that

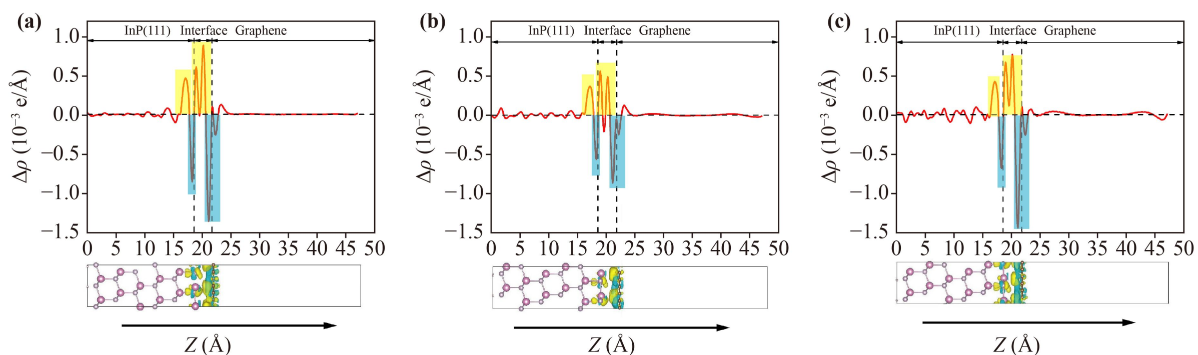

Fig. 4 The charge density difference and corresponding planar-average electron density difference. **(a)** Configuration A, **(b)** configuration B, **(c)** configuration C. The isosurfaces of charge density are set to be 3×10^{-4} Å^{-3}. The yellow color represents the charge accumulation, while the cyan color represents charge depletion.

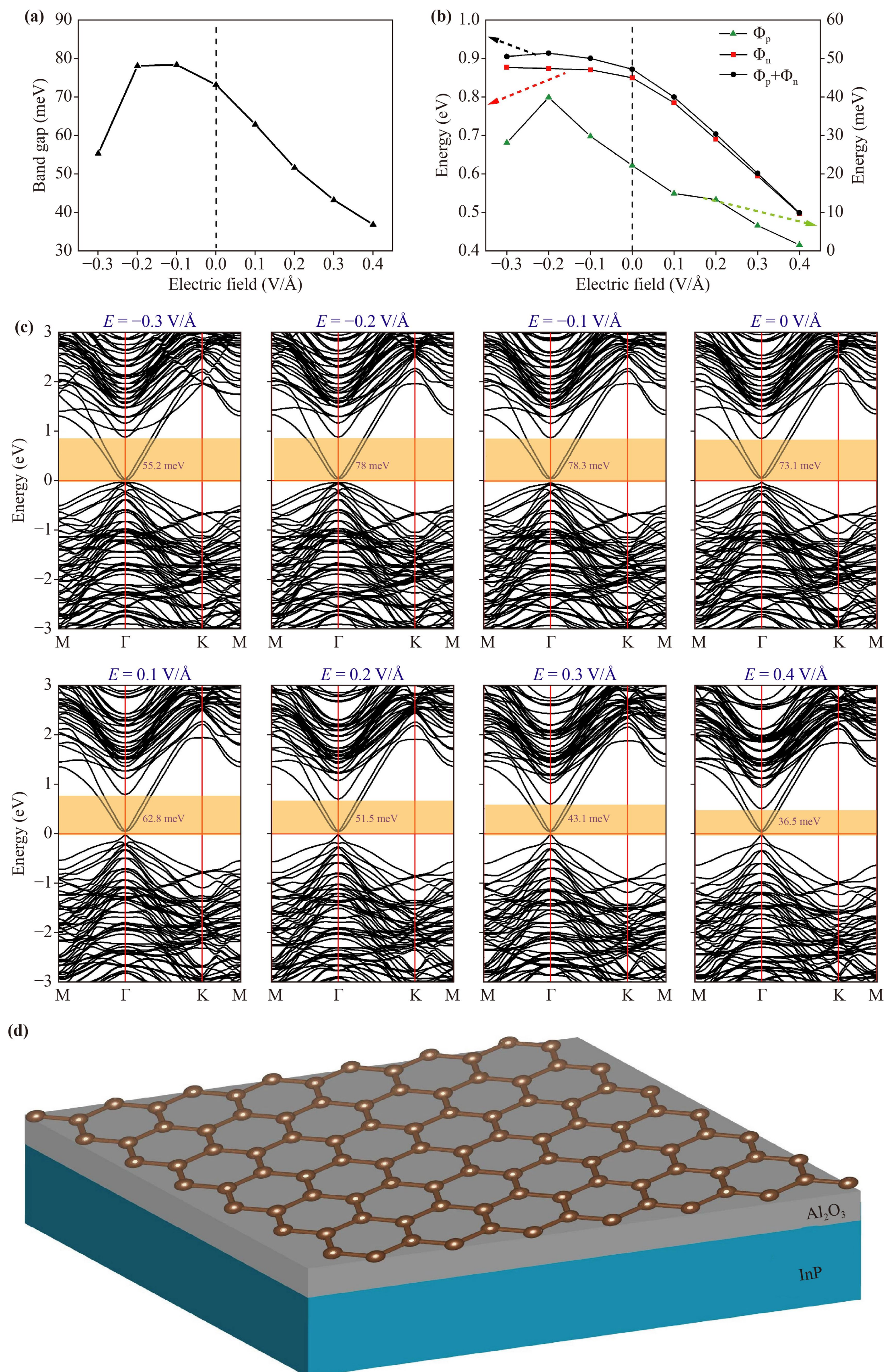

Fig. 5 The change of **(a)** opened band gap of graphene in graphene/InP, **(b)** Schottky barrier height and **(c)** band structure for the configuration A as a function of the external electric field. **(d)** Schematic structure of Graphene/Al_2O_3/InP heterostructure.

Φ_n decreases significantly with increasing positive electric field, but it almost keeps constant for negative electric field. The underlying physical mechanism of such a tunability of SBH Φ_n can be explained by the compensation of the built-in electric field by the positive external electric field. Moreover, one can find that Φ_p in configurations A decreases with increasing the positive external electric field, while it increases slowly first and then decreases. The trend of p-type Schottky barrier is consistent with that of band gap of graphene in graphene/InP heterostructure for configuration A. Also, the total SBH ($\Phi_n + \Phi_p$), nearly consistent with the band gap of the InP slab, can be tuned by the external electric field, as shown in the black filled pentagon of Fig. 5(b). These results originate from electrical tunability of a weak hybridization between the π^* band of graphene and valence band edge of InP slab. Interestingly, the band structures in Fig. 5(c) reveal that the heterostructure still keeps a p-type Schottky contact with a relatively low SBH when the value of the external electric field ranges widely from –0.3 to 0.4 V/Å. This result explains why the PCE of graphene/InP heterojunction is so small, which is 5.6% [29]: the relatively low p-type SBH induced by the contact between bulk InP semiconductor and graphene in Schottky devices seriously leads to a degradation of photoelectronic device's performance [48]. In order to achieve high PCE in graphene/InP heterostructure solar cells, the SBH must be increased. Therefore, a graphene/Al_2O_3/InP heterostructure is proposed to raise SBH [49], as shown in Fig. 5(d). Al_2O_3 is a high-k dielectric material that acts as a passivation layer depositing on InP surface, which not only reduce the influence of the surface defects but also increase the SBH. If a oxide layer is present between graphene and InP slab, the insulating barrier causes electron-transport/hole-blocking, which is well explained as asymmetric tunneling between electrons and holes [49]. The PCE of graphene/InP solar cell will be expected to improve.

4 Conclusion

In conclusion, we have found three possible configurations of graphene/InP heterostructures and systematically investigated their electronic properties as well as the effect of external electric fields on the electronic properties using DFT calculations. Due to the weak interlayer vdW interaction, the electronic properties of the alone graphene and InP slab are mostly preserved in the heterostructures. Graphene in three configurations is opened up a band gap of 73.1 meV, 170.9 meV, and 81.3 meV, respectively. Meanwhile, the charge density difference reveals a p-type Schottky contact of InP with graphene, and thus a built-in electric field occurs near the interface and points to InP slab from graphene, which can boost the separation of photogenerated electron-hole pairs in graphene/InP solar cells. However, SBH of this p-type contact is low, leading to a low PCE of graphene/InP solar cells. A new heterostructure of graphene/Al_2O_3/InP has been proposed to increase SBH and PCE. It is also found that opened band gaps of graphene and SBH in graphene/InP heterostructure can be significantly tuned by an external electric field, which may be useful for the applications of graphene/InP photodetectors. Our results provide a valuable theoretical understanding to comprehend the interfacial interaction between graphene and InP(111) and an important guidance for improving the performance of devices based on graphene/InP vdW heterostructure.

Acknowledgements This work was supported by the National Natural Science Foundation of China (Grant Nos. 12074441, 11774438, and 12104518) and Guangdong Basic and Applied Basic Foundation in China (Grant No. 2019A1515011572 and 2022A1515012643).

References

1. A. K. Geim, Graphene: Status and prospects, *Science* 324(5934), 1530 (2009)
2. K. Chen, M. N. Yogeesh, Y. Huang, S. Q. Zhang, F. He, X. H. Meng, S. Y. Fang, N. Sheehan, T. H. Tao, S. R. Bank, J. F. Lin, D. Akinwande, P. Sutter, T. S. Lai, and Y. G. Wang, Non-destructive measurement of photoexcited carrier transport in graphene with ultrafast grating imaging technique, *Carbon* 107, 233 (2016)
3. S. Bae, H. Kim, Y. Lee, X. Xu, J. S. Park, Y. Zheng, J. Balakrishnan, T. Lei, H. Ri Kim, Y. I. Song, Y. J. Kim, K. S. Kim, B. Özyilmaz, J. H. Ahn, B. H. Hong, and S. Iijima, Roll-to-roll production of 30-inch graphene films for transparent electrodes, *Nat. Nanotechnol.* 5(8), 574 (2010)
4. A. A. Balandin, S. Ghosh, W. Z. Bao, I. Calizo, D. Teweldebrhan, F. Miao, and C. N. Lau, Superior thermal conductivity of single-layer graphene, *Nano Lett.* 8(3), 902 (2008)
5. A. K. Geim and K. S. Novoselov, The rise of graphene, *Nat. Mater.* 6(3), 183 (2007)
6. G. Gui, J. Li, and J. Zhong, Band structure engineering of graphene by strain: First-principles calculations, *Phys. Rev. B* 78(7), 075435 (2008)
7. J. B. Oostinga, H. B. Heersche, X. L. Liu, A. F. Morpurgo, and L. M. K. Vandersypen, Gate-induced insulating state in bilayer graphene devices, *Nat. Mater.* 7(2), 151 (2008)
8. D. B. Zhang, Y. Hu, H. X. Zhong, S. J. Yuan, and C. Liu, Effects of out-of-plane strains and electric fields on the electronic structures of graphene/MTe (M = Al, B) heterostructures, *Nanoscale* 11(29), 13800 (2019)
9. S. Singh, C. Espejo, and A. H. Romero, Structural, electronic, vibrational, and elastic properties of graphene/MoS_2 bilayer heterostructures, *Phys. Rev. B* 98(15), 155309 (2018)
10. K. Zollner, M. Gmitra, and J. Fabian, Heterostructures of graphene and hBN: Electronic, spin–orbit, and spin

relaxation properties from first principles, *Phys. Rev. B* 99(12), 125151 (2019)

11. M. Gmitra, D. Kochan, P. Högl, and J. Fabian, J. and Fabian, Trivial and inverted Dirac bands and the emergence of quantum spin Hall states in graphene on transition-metal dichalcogenides, *Phys. Rev. B* 93(15), 155104 (2016)
12. X.-R. Hu, J.-M. Zheng, Z.-Y. Ren, Strong interlayer coupling in phosphorene/graphene van der Waals heterostructure: A first-principles investigation, *Front. Phys.* 13, 137302 (2018)
13. L. Zhang, L. Fan, Z. Li, E. Shi, X. M. Li, H. B. Li, C. Y. Ji, Y. Jia, J. Q. Wei, K. L. Wang, H. W. Zhu, D. H. Wu, and A. Y. Cao, Graphene-CdSe nanobelt solar cells with tunable configurations, *Nano Res.* 4(9), 891 (2011)
14. W. J. Jie, F. G. Zheng, and J. H. Hao, Graphene/gallium arsenide-based Schottky junction solar cells, *Appl. Phys. Lett.* 103(23), 233111 (2013)
15. C. Y. Lan, C. Li, S. Wang, T. Y. He, Z. F. Zhou, D. P. Wei, H. Y. Guo, H. Yang, and Y. Liu, Highly responsive and broadband photodetectors based on WS_2–graphene van der Waals epitaxial heterostructures, *J. Mater. Chem. C* 5(6), 1494 (2017)
16. D. Pierucci, H. Henck, J. Avila, A. Balan, C. H. Naylor, G. Patriarche, Y. J. Dappe, M. G. Silly, F. Sirotti, A. T. C. Johnson, M. C. Asensio, and A. Ouerghi, Band alignment and minigaps in monolayer MoS_2–graphene van der Waals heterostructures, *Nano Lett.* 16(7), 4054 (2016)
17. J. A. Miwa, M. Dendzik, S. S. Gronborg, M. Bianchi, J. V. Lauritsen, P. Hofmann, and S. Ulstrup, Van der Waals epitaxy of two-dimensional MoS_2-graphene heterostructures in ultrahigh vacuum, *ACS Nano* 9(6), 6502 (2015)
18. H. Büch, A. Rossi, S. Forti, D. Convertino, V. Tozzini, and C. Coletti, Superlubricity of epitaxial monolayer WS_2 on graphene, *Nano Res.* 11(11), 5946 (2018)
19. M. L. Sun, J. P. Chou, Q. Q. Ren, Y. M. Zhao, J. Yu, and W. C. Tang, Tunable Schottky barrier in van der Waals heterostructures of graphene and g-GaN, *Appl. Phys. Lett.* 110(17), 173105 (2017)
20. S. Tongay, M. Lemaitre, T. Schumann, K. Berke, B. R. Appleton, B. Gila, and A. F. Hebard, Graphene/GaN Schottky diodes: Stability at elevated temperatures, *Appl. Phys. Lett.* 99(10), 102102 (2011)
21. D. P. Andrade, R. H. Miwa, and G. P. Srivastava, Graphene and graphene nanoribbons on InAs(110) and Au/InAs(110) surfaces: An *ab initio* study, *Phys. Rev. B* 84(16), 165322 (2011)
22. Y. J. Hong, J. W. Yang, W. H. Lee, R. S. Ruoff, K. S. Kim, and T. Fukui, Van der Waals epitaxial double heterostructure: InAs/single-layer graphene/InAs, *Adv. Mater.* 25(47), 6847 (2013)
23. I. Vurgaftman, J. R. Meyer, and L. R. Ram-Mohan, Band parameters for III–V compound semiconductors and their alloys, *J. Appl. Phys.* 89(11), 5815 (2001)
24. J. J. Loferski, Theoretical considerations governing the choice of the optimum semiconductor for photovoltaic solar energy conversion, *J. Appl. Phys.* 27(7), 777 (1956)
25. X. M. Li, H. W. Zhu, K. L. Wang, A. Y. Cao, J. Q. Wei, C. Y. Li, Y. Jia, Z. Li, X. Li, and D. H. Wu, Graphene-on-silicon Schottky junction solar cells, *Adv. Mater.* 22(25), 2743 (2010)
26. X. Miao, S. Tongay, M. K. Petterson, K. Berke, A. G. Rinzler, B. R. Appleton, and A. F. Hebard, High efficiency graphene solar cells by chemical doping, *Nano Lett.* 12(6), 2745 (2012)
27. X. Q. Li, W. C. Chen, S. J. Zhang, Z. Q. Wu, P. Wang, Z. J. Xu, H. S. Chen, W. Y. Yin, H. K. Zhong, and S. S. Lin, 18.5% efficient graphene/GaAs van der Waals heterostructure solar cell, *Nano Energy* 16, 310 (2015)
28. A. Yamamoto, M. Yamaguchi, and C. Uemura, High conversion efficiency and high radiation resistance InP homojunction solar cells, *Appl. Phys. Lett.* 44(6), 611 (1984)
29. P. Wang, X. Q. Li, Z. J. Xu, Z. Q. Wu, S. J. Zhang, W. L. Xu, H. K. Zhong, H. S. Chen, E. P. Li, J. K. Luo, Q. K. Yu, and S. S. Lin, Tunable graphene/indium phosphide heterostructure solar cells, *Nano Energy* 13, 509 (2015)
30. X. F. Lu, L. X. Li, X. Guo, J. Q. Ren, H. T. Xue, and F. L. Tang, Effects of vertical strain and electric field on the electronic properties and interface contact of graphene/InP vdW heterostructure, *Comput. Mater. Sci.* 198, 110677 (2021)
31. T. Zhang and J. Chen, Graphene/InP Schottky junction near-infrared photodetectors, *Appl. Phys. A* 126(11), 832 (2020)
32. P. E. Blöchl, Projector augmented-wave method, *Phys. Rev. B* 50(24), 17953 (1994)
33. G. Kresse and J. Furthmuller, Efficient iterative schemes for *ab initio* total-energy calculations using a plane-wave basis set, *Phys. Rev. B* 54(16), 11169 (1996)
34. J. P. Perdew, K. Burke, and M. Ernzerhof, Generalized gradient approximation made simple, *Phys. Rev. Lett.* 77(18), 3865 (1996)
35. S. Grimme, Semiempirical GGA-type density functional constructed with a long-range dispersion correction, *J. Comput. Chem.* 27(15), 1787 (2006)
36. F. Ortmann, F. Bechstedt, and W. G. Schmidt, Semiempirical van der Waals correction to the density functional description of solids and molecular structures, *Phys. Rev. B* 73(20), 205101 (2006)
37. S. Kalvoda, B. Paulus, P. Fulde, and H. Stoll, Influence of electron correlations on ground-state properties of III-V semiconductors, *Phys. Rev. B* 55(7), 4027 (1997)
38. V. L. Bekenev and S. M. Zubkova, Electronic structure of the CdTe(111) A-(2 $\times$ 2) surface, *Phys. Solid State* 57(9), 1878 (2015)
39. K. Shiraishi, A new slab model approach for electronic structure calculation of polar semiconductors surface, *J. Phys. Soc. Jpn.* 59(10), 3455 (1990)
40. P. W. Tasker, The stability of ionic crystal surfaces, *J. Phys. C* 12(22), 4977 (1979)
41. Y. Horio, J. Yuhara, Y. Takakuwa, Structural analysis of an InP(111) A surface using reflection high-energy electron diffraction rocking curves, *Jpn. J. Appl. Phys.* 58, SIIA14 (2019)
42. T. Akiyama, T. Kondo, H. Tatematsu, K. Nakamura, and T. Ito, *Ab initio* approach to reconstructions of the InP(111)A surface: Role of hydrogen atoms passivating surface dangling bonds, *Phys. Rev. B* 78(20), 205318

(2008)
43. M. D. Pashley, Electron counting model and its application to island structures on molecular-beam epitaxy grown GaAs(001) and ZnSe(001), *Phys. Rev. B* 40(15), 10481 (1989)
44. M. Farjam and H. Rafii-Tabar, Energy gap opening in submonolayer lithium on graphene: Local density functional and tight-binding calculations, *Phys. Rev. B* 79, 045417 (2009)
45. H. T. T. Nguyen, M. M. Obeid, A. Bafekry, M. Idrees, T. V. Vu, H. V. Phuc, N. N. Hieu, L. Hoa, B. Amin, and C. V. Nguyen, Interfacial characteristics, Schottky contact, and optical performance of a graphene/Ga_2SSe van der Waals heterostructure: Strain engineering and electric field tunability, *Phys. Rev. B* 102(7), 075414 (2020)
46. J. Bardeen, Surface states and rectification at a metal semi-conductor contact, *Phys. Rev.* 71(10), 717 (1947)
47. Q. Liu, J. J. Li, D. Wu, X. Q. Deng, Z. H. Zhang, Z. Q. Fan, and K. Q. Chen, Gate-controlled reversible rectifying behavior investigated in a two-dimensional MoS_2 diode, *Phys. Rev. B* 104(4), 045412 (2021)
48. F. E. Cimilli Çatir, Properties of a facile growth of spray pyrolysis-based rGO films and device performance for Au/rGO/n-InP Schottky diodes, *J. Mater. Sci-Mater. Electron.* 32, 611 (2021)
49. M. A. Rehman, I. Akhtar, W. Choi, K. Akbar, A. Farooq, S. Hussain, M. A. Shehzad, S. H. Chun, J. Jung, and Y. Seo, Influence of an Al_2O_3 interlayer in a directly grown graphene-silicon Schottky junction solar cell, *Carbon* 132, 157 (2018)